Supplement to: Sixteen years of MOPITT satellite data strongly constrain Amazon CO fire emissions

Stijn Naus[1,2], Lucas G. Domingues[3,4], Maarten Krol[1,5], Ingrid T. Luijkx[1], Luciana V. Gatti[4,6], John B. Miller[7], Emanuel Gloor[8], Sourish Basu[9,10], Caio Correia[4,6], Gerbrand Koren[1], Helen M. Worden[11], Johannes Flemming[12], Gabrielle Pétron[7,13], and Wouter Peters[1,14]

[1]Meteorology and Air Quality, Wageningen University and Research, The Netherlands
[2]SRON Netherlands Institute for Space Research, Utrecht, The Netherlands
[3]National Isotope Centre, GNS Science, New Zealand
[4]Nuclear and Energy Research Institute, São Paulo, Brazil
[5]Institute for Marine and Atmospheric Research, Utrecht University, The Netherlands
[6]National Institute for Space Research (INPE), São José dos Campos, Brazil
[7]Global Monitoring Laboratory, National Oceanographic and Atmospheric Administration, Boulder, CO, USA
[8]School of Geography, University of Leeds, Leeds, UK
[9]Earth System Science Interdisciplinary Center, University of Maryland, MD, USA
[10]NASA Goddard Space Flight Center, Greenbelt, MD, USA.
[11]Atmospheric Chemistry Observations and Modeling, National Center for Atmospheric Research, Boulder, CO, USA
[12]European Centre for Medium-Range Weather Forecasts (ECMWF), Reading, UK
[13]Cooperative Institute for Research in Environmental Sciences, University of Colorado, Boulder, CO, USA
[14]Centre for Isotope Research, University of Groningen, The Netherlands

Correspondence: Stijn Naus (s.naus@sron.nl)

S1 Comparison between simulated and observed NOAA surface observations

Since we assimilate satellite observations only over the South-American zoom domains, global CO emissions and by extent South-American boundary conditions are constrained by flask observations sampled at NOAA background sites. We assimilated all NOAA surface sites for which CO data are available, which amounts to 37−44 sites, depending on the year. Typically, 3–4 observations per site, per month are available, for a global total of 100−150 observations per month. We used a fixed measurement uncertainty of 2 ppb CO for surface observations in the inverse system.

In Fig. S1, the difference between simulated and observed CO mole fractions is shown at four representative surface sites, for 2010–2016. The comparison looks similar for the entire 2003–2018 period, but because the sensitivity inversion only includes 2010, 2015 and 2016, we zoom in on the 2010–2016 period. Alert (ALT) is a high-altitude Northern Hemispheric site, and, after optimization, mole fractions at ALT are very well reproduced, except for a spin-up period. The optimization works less well for the other three sites, which are located closer to the zoom domains. In the optimization, there is a trade-off between improving the match with surface observations and improving the match with satellite observations that is particularly important near the South-American zoom domains, where coverage of surface observations and satellite CO columns partly overlap. Because there are many more satellite observations (around 10.000 per day) compared to surface observations (3-4

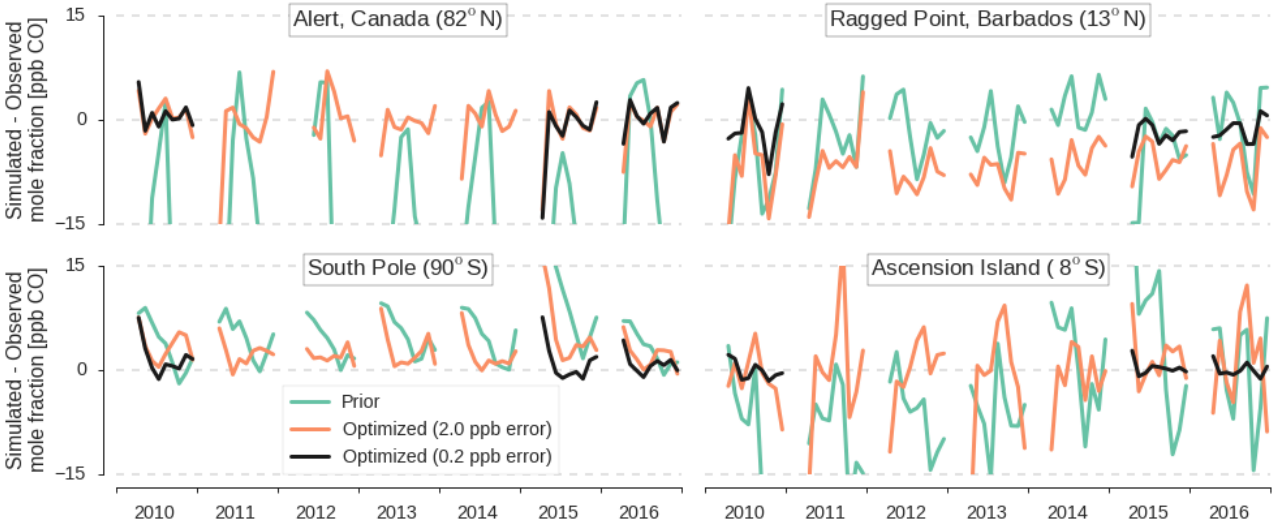

Figure S1. Timeseries of the difference between simulated and observed monthly mean CO mole fractions at four NOAA surface sites. Shown are results before optimization (green), after optimization in our standard inversion set-up with an observational error of 2.0 ppb per sample (orange), and after optimization in an inversion where the observational error was reduced to 0.2 ppb (black; only for 2010, 2015 and 2016).

per month, per site), satellite observations are weighted more heavily than surface observations. We have tried to reduce this effect by inflating the error on satellite observations by a factor $\sqrt{50}$ (as in Nechita-Banda et al. (2018)), but near the zoom domain satellite observations still seem to dominate. This can be seen from the relative good match at ALT (and most other sites; not shown) compared to the other three sites shown in Fig. S1. Especially Ragged Point, Barbados (RPB) and Ascension Island (ASC) are important for the inversion, since these sites roughly represent the inflow conditions of the Amazon domain (e.g. Gatti et al., 2014). The posterior differences between simulated and observed mole fractions at these sites fall outside the prescribed observational uncertainties for surface data and, especially at RPB, are not always an improvement on the prior simulation.

To investigate the importance of our difficulty in reproducing mole fractions at surface sites near the zoom domain, we performed inversions for 2010, 2015 and 2016, in which we reduced the error on CO surface observations from 2 ppb to 0.2 ppb. As expected, in these new inversions the agreement with observations at all sites improves compared to our standard inversions (black lines in Fig. S1), while MOPITT CO columns in these three new inversions are reproduced equally well as in our standard inversions (not shown). Biomass burning emissions derived in these three inversions are lower than those derived in our standard inversions (Fig. S2), but the difference is small and consistent between years ($7-11$ Tg/year). We note that this is consistent with the posterior mismatch at RPB (orange line in Fig. S1). Namely, the simulated mole fractions at RPB are consistently too low in our standard inversions, while in the inversions with a 0.2 ppb error simulated mole fractions at RPB

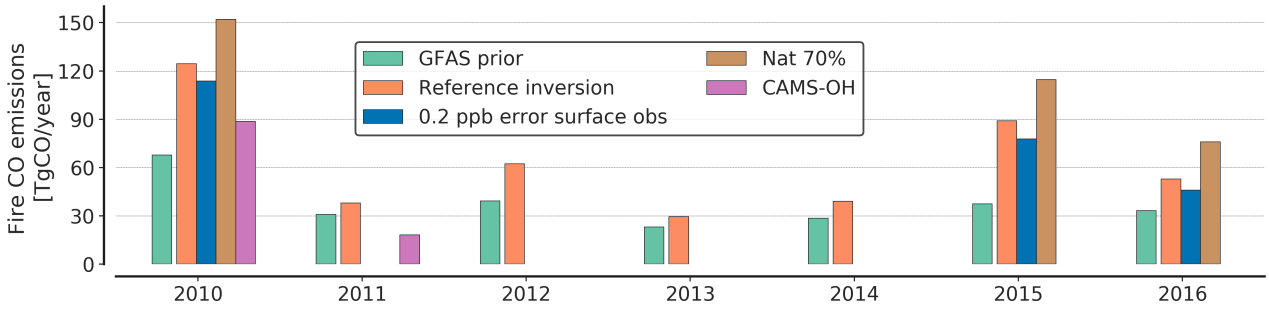

Figure S2. Total CO emissions from biomass burning summed over the 1° x 1° South-American zoom domain, and over the April − December inversion period. Results for four sets of inversions are shown, which each started from the GFAS fire prior, and they all were optimized with MOPITT satellite data. The first is the default inversion (performed for all years). In the second inversion the assumed error on NOAA surface observations was reduced from 2.0 ppb to 0.2 ppb (performed for 2010, 2015 and 2016; described in Sup. SS1). For the third inversion, the natural production of CO was scaled down to 70% of the original value (performed for 2010, 2015 and 2016; see also Fig S3 and Sup. S2.1). In the fourth inversion, the default, climatological OH fields (based on Spivakovsky et al. (2000) and Brühl and Crutzen (1993); see also Methods of main text) were replaced by interannual varying OH fields from the CAMS reanalysis (performed for 2010 and 2011; described in Sup. S2.2).

are higher, which results in more inflow of CO into the Amazon domain and consequently lower local emissions derived in the inversion.

Notably, RPB is located inside the 3° x 2° zoom domain, i.e. satellite observations are assimilated over this site (see Fig. 1 in main manuscript). Therefore, the interannual consistency of the posterior bias at RPB (orange line in Fig. S1) can be compared to the aircraft profiles at Santarém, where simulated mole fractions are also too low, even though MOPITT CO columns are reproduced well over the same area (see Supp. S3 and Fig. S5). The similarity between these offsets suggest either a systematic bias in the MOPITT CO columns, or systematic uncertainties in the vertical transport of TM5, since the vertical sensitivity of MOPITT CO columns, of surface observations and of aircraft profiles are all different. In previous work, this issue was partly addressed by co-optimizing a latitudinally dependent bias correction to MOPITT CO columns (Hooghiemstra et al., 2012). However, as long as the offsets are relatively constant interannually, the conclusions we draw in the main text are not significantly affected.

Assimilating NOAA surface observations in our inversion helps to derive a consistent global picture and the poor match between simulated and observed mole fractions at sites near the Amazon domain seems worrying. However, the inversions with a 0.2 ppb observational error show that we can simultaneously reproduce surface observations and MOPITT CO columns with approximately the same biomass burning emissions as in the standard inversions. This indicates a limited sensitivity of derived emissions to the boundary conditions. Intuitively, this can be understood, since, during the dry season, advection of CO into the Amazon domain is less important than local emissions. In conclusion, we find some inconsistencies in the

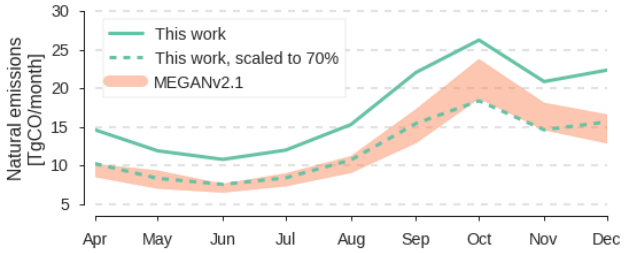

Figure S3. Timeseries of monthly total biogenic CO emissions inside the 1° x 1° South-American zoom domain. The climatological natural emissions used in this study (green solid), as well as the same estimate uniformly scaled to 70% (green dashed) are both shown. Additionally, natural emissions based on the MEGANv2.1 inventory (Sindelarova et al., 2014) are shown as one standard deviation spread around the 2003−2018 mean (shaded orange). Since the MEGANv2.1 inventory only provides direct biogenic CO emissions and emissions of CO precursors, we have used CO production calculated in simulations described in Zheng et al. (2019), in which precursor emissions from MEGANv2.1 were used to derive secondary production of CO.

Amazon boundary conditions in our standard inversions, but we also find limited sensitivity of derived emissions to these inconsistencies.

S2 Other sensitivities in the inverse system

In our main text, we have presented the sensitivity of derived fire emissions to fire emission prior, and to assimilating IASI instead of MOPITT satellite data. In this supplement, we discuss sensitivities of the derived CO emissions to the other important components of the inverse system: CO production from NMHC and OH chemistry. In general, we find that the absolute magnitude of the derived CO emissions, and the spatio-temporal patterns therein, are robust.

S2.1 CO production from NMVOC

In this section we investigate the influence of natural CO emissions on our derived fire emissions. The aggregated category of natural emissions as defined here includes secondary production of CO (from CH_4 and NMVOCs), and direct biogenic CO emissions. This source category partly correlates with fire emissions, as CO production from NMVOCs in particular peaks during the dry season, because of significant NMVOC emissions from fires, as well as higher biogenic emissions of natural emitted NMVOCs like isoprene during dry months.

The natural emissions used in our standard emissions were annually repeating and retrieved from a full-chemistry simulation of TM5 for 2006. While we consider the spatio-temporal patterns of this distribution realistic, the absolute amount of natural CO emissions was very high. Globally, 1750 Tg CO/year is emitted in this aggregated category, compared to, for example, 1400 Tg/year suggested in Huijnen et al. (2010). When we compare our natural CO emissions with CO emissions calculated based on the Model of Emissions of Gases and Aerosols from Nature (MEGANv2.1)(Sindelarova et al., 2014), we find confirmation that

our reference estimate of natural emissions is too high (Fig. S3). Therefore, as a sensitivity test, we have performed inversions with natural emissions scaled down by 30% (green dashed line in Fig. S3), which is more in line with other estimates.

In the inversions where natural emissions have been scaled down, we derive higher biomass burning emissions (Fig. S2). The difference between biomass burning emissions derived in the two inversions is 23-27 Tg/year, while natural emissions are scaled down by 47 Tg/year. In other words, a systematic bias in natural emissions of 1 Tg translates to approximately a 0.5 Tg bias in biomass burning emissions. We can compare this sensitivity to the interannual variability in CO production derived from MEGANv2.1. The difference between natural emissions in the highest and lowest year is 30 Tg/year, which translates to a maximum uncertainty in biomass burning emissions of $\sim$15 TgCO/year.

Given these results, we consider natural emissions to be one of the most important uncertainties in our inverse system. Since we used high natural emissions in our standard inversions, the biomass burning emissions we have derived might be on the low side. We note that our sensitivity inversions show that systematic errors in natural emissions mostly translate to systematic errors in biomass burning emissions, i.e. the interannual variability of our estimates remains unaffected. However, natural emissions do undergo interannual variability, albeit less so than biomass burning. We conservatively estimate an error in the interannual variability of derived CO emissions of $10-15$ TgCO/year related to natural emissions. On the other hand, in Section 3.3.2 we show that biomass burning emissions derived in a different inverse system that used natural emissions from the MEGANv2.1 inventory are very similar to those derived in this study. This suggests that, ultimately, the uncertainty related to natural emissions can be cancelled out by other uncertainties.

S2.2 OH chemistry fields

The final uncertainty in the CO budget that we consider is loss to oxidation by OH. Since OH has a lifetime of seconds, its atmospheric abundance is determined by local atmospheric conditions, which can be disturbed by high emissions from fires: precisely our regime of interest. Our default OH field (from Spivakovsky et al. (2000) in the troposphere, scaled by a factor 0.92; from Brühl and Crutzen (1993) in the stratosphere) is climatological, and it therefore does not include the interannual disturbances in fire emissions. Since CO has a typical atmospheric lifetime of one month, variations in OH will drive an integrated, slow response in atmospheric CO abundance, which suggests that the impact of varying OH on emission localization and timing will be small. However, if we systematically over- or underestimate OH abundance, then this can cause a significant, possibly interannually varying bias in our CO emission estimates. To test the sensitivity of our results to the OH fields used, we performed inversions for 2010 and 2011 with daily OH fields from the reanalysis product released by the Copernicus Atmosphere Monitoring Service (CAMS) (Inness et al., 2019).

In inversions with CAMS OH fields, we find lower biomass burning emissions by 35 Tg and 19 Tg in 2010 and 2011 respectively (Fig. S2). This is one of the largest sensitivities in our inverse system with significant interannual variability. It is driven by the large difference between the two different OH fields we have tested: in some regions CAMS OH is lower than our default OH fields by a factor 100 (Fig. S4). This difference is largely consistent between months and between years.

The gap in OH fields over remote forests is a known attribute of OH fields derived in some full-chemistry models and it is likely related to incomplete recycling mechanisms for OH. In-situ measurements of OH over remote forests have revealed

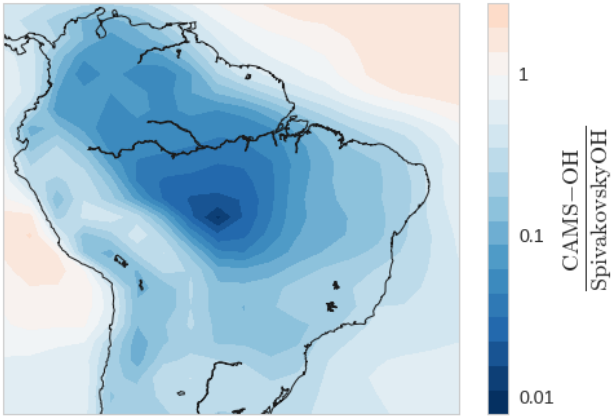

Figure S4. The ratio between OH fields from the CAMS reanalysis product for 2010, and climatological OH fields from Spivakovsky et al. (2000), scaled by 0.92. OH fields were first averaged over our April−December inversion window and over the lowest 10 model layers, corresponding to approximately 500 hPa, or 5 km. The color scale is logarithmic.

higher OH concentrations, even under low-NO_x conditions (Lelieveld et al., 2008). One explanation is that under these pristine conditions, isoprene oxidation can sustain a high OH recycling efficiency (e.g. Lelieveld et al., 2008; Taraborrelli et al., 2012), although more recent work has suggested that natural NO_x emissions have been underestimated over these regions (Wells et al., 2020). Whatever the driving mechanism, the gap in OH over the Amazon in CAMS-OH could explain why, in the CAMS reanalysis for CO (Flemming et al., 2017), GFAS emissions do not result in an underestimate of CO over the Amazon: too-low OH and too-low fire emissions cancel out.

Given these considerations, we deem our climatological OH fields more realistic over the Amazon region than the OH fields from the CAMS reanalysis. The large sensitivity of derived emissions to the OH field used is likely a reflection of the extreme difference between the OH fields we have tested, rather than a reflection of a large intrinsic sensitivity in the inverse system. We note that OH variations have a relatively diffuse, slow impact on CO, which means that its contribution to the sharp dry season peak in atmospheric CO abundance is limited. However, loss to OH does contribute substantially to the Amazon CO budget, and efforts to understand and constrain OH over remote regions (e.g. Fu et al., 2019; Nölscher et al., 2016) will translate to better biomass burning estimates. For example, in Nechita-Banda et al. (2018) it was found that pollutant emissions from fires reduced OH concentrations, and including this effect in the inversion reduced the estimated CO fire emissions by $\sim 7\%$. We do note that the fire source in their study, which was focused on Indonesia, included large peat fires that emit relatively low amounts of NO_x, so that the impact on OH concentrations is relatively high, compared to savanna or forest fires that dominate in the Amazon domain.

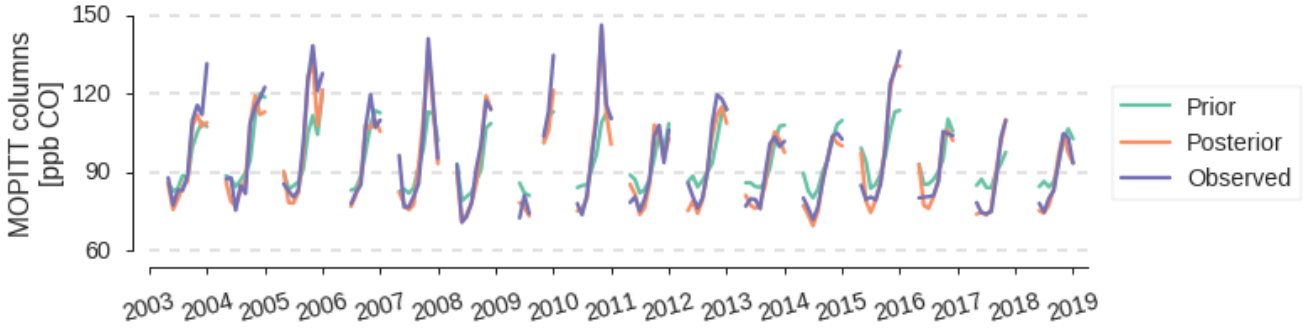

Figure S5. Simulated and observed monthly mean MOPITT CO columns over the Santarém aircraft site. Columns are averaged over a 1° by 1° area centered on Santarém (56°E; 2.8°S). CO columns sampled from the prior (green) and from the posterior (orange) simulation are shown.

S3 CO columns over the Santarém aircraft site

Out of the five sites for which aircraft profiles are compared to model results, we only found substantial differences between observed and TM5-simulated aircraft profiles at the Santarém aircraft site. Specifically, aircraft profiles sampled in a simulation with MOPITT-optimized emissions were systematically too low (Figure 2 in the main text). In contrast, MOPITT CO columns over Santarém are well reproduced (Figure S5). This effect is similar to what we observed at the NOAA surface site of Ragged Point, Barbados, where simulated CO mole fractions in the standard inversion were also lower than those observed (Supp. S1). This could point to a systematic bias in the MOPITT CO columns. However, surface observations, aircraft profiles and MOPITT CO columns all have different vertical sensitivities and therefore systematic uncertainties in the vertical transport of TM5 also affect this comparison.

References

C. Brühl and P. J. Crutzen. MPIC two-dimensional model. *NASA Ref. Publ*, 1292:103–104, 1993.

J. Flemming, A. Benedetti, A. Inness, R. J. Engelen, L. Jones, V. Huijnen, S. Remy, M. Parrington, M. Suttie, A. Bozzo, V.-H. Peuch, D. Akritidis, and E. Katragkou. The CAMS interim Reanalysis of Carbon Monoxide, Ozone and Aerosol for 2003–2015. *Atmospheric Chemistry and Physics*, 17(3):1945–1983, 2017. https://doi.org/10.5194/acp-17-1945-2017. URL https://acp.copernicus.org/articles/17/1945/2017/.

D. Fu, D. B. Millet, K. C. Wells, V. H. Payne, S. Yu, A. Guenther, and A. Eldering. Direct retrieval of isoprene from satellite-based infrared measurements. *Nature communications*, 10(1):1–12, 2019.

L. V. Gatti, M Gloor, J. B. Miller, C. E. Doughty, Y Malhi, L. G Domingues, L. S Basso, A Martinewski, C S C Correia, V F Borges, S. Freitas, R. Braz, L. O. Anderson, H. Rocha, J. Grace, O. L. Phillips, and J. Lloyd. Drought sensitivity of Amazonian carbon balance revealed by atmospheric measurements. *Nature*, 506(7486):76, 2014.

P. B. Hooghiemstra, M. C. Krol, T. T. van Leeuwen, G. R. van der Werf, P. C. Novelli, M. N. Deeter, I. Aben, and T. Röckmann. Interannual variability of carbon monoxide emission estimates over South America from 2006 to 2010. *Journal of Geophysical Research: Atmospheres*, 117(D15), 2012. https://doi.org/10.1029/2012JD017758. URL https://agupubs.onlinelibrary.wiley.com/doi/abs/10.1029/2012JD017758.

V. Huijnen, J. Williams, M. van Weele, T. van Noije, M. C. Krol, F. Dentener, A. Segers, S. Houweling, W. Peters, J. de Laat, F. K. Boersma, P. Bergamaschi, P. van Velthoven, P. Le Sager, H. Eskes, F. Alkemade, R. Scheele, P. Nédélec, and H.-W. Pätz. The global chemistry transport model TM5: description and evaluation of the tropospheric chemistry version 3.0. *Geoscientific Model Development*, 3(2): 445–473, 2010.

A. Inness, M. Ades, A. Agustí-Panareda, J. Barré, A. Benedictow, A.-M. Blechschmidt, J. J. Dominguez, R. Engelen, H. Eskes, J. Flemming, V. Huijnen, L. Jones, Z. Kipling, S. Massart, M. Parrington, V.-H. Peuch, M. Razinger, S. Remy, M. Schulz, and M. Suttie. The CAMS reanalysis of atmospheric composition. *Atmospheric Chemistry and Physics*, 19(6):3515–3556, 2019. https://doi.org/10.5194/acp-19-3515-2019. URL https://acp.copernicus.org/articles/19/3515/2019/.

J. Lelieveld, T. M. Butler, J. N. Crowley, T. J. Dillon, H. Fischer, L. Ganzeveld, H. Harder, M. G. Lawrence, M. Martinez, D. Taraborrelli, and J. Williams. Atmospheric oxidation capacity sustained by a tropical forest. *Nature*, 452(7188):737–740, 2008.

N. Nechita-Banda, M. Krol, G. R. Van Der Werf, J. W. Kaiser, S. Pandey, Vincent Huijnen, Cathy Clerbaux, Pierre Coheur, Merritt N Deeter, and Thomas Röckmann. Monitoring emissions from the 2015 Indonesian fires using CO satellite data. *Philosophical Transactions of the Royal Society B: Biological Sciences*, 373(1760):20170307, 2018.

A. C. Nölscher, A. M. Yañez-Serrano, S. Wolff, A. C. De Araujo, J. V. Lavrič, J. Kesselmeier, and J Williams. Unexpected seasonality in quantity and composition of Amazon rainforest air reactivity. *Nature communications*, 7(1):1–12, 2016.

K. Sindelarova, C. Granier, I. Bouarar, A. Guenther, S. Tilmes, T. Stavrakou, J.-F. Müller, U. Kuhn, P. Stefani, and W. Knorr. Global data set of biogenic voc emissions calculated by the megan model over the last 30 years. *Atmospheric Chemistry and Physics*, 14(17):9317–9341, 2014. https://doi.org/10.5194/acp-14-9317-2014. URL https://acp.copernicus.org/articles/14/9317/2014/.

C. M. Spivakovsky, J. A. Logan, S. A. Montzka, Y. J. Balkanski, M. Foreman-Fowler, D. B. A. Jones, L. W. Horowitz, A. C. Fusco, C. A. M. Brenninkmeijer, M. J. Prather, S. C. Wofsy, and M. B. McElroy. Three-dimensional climatological distribution of tropospheric OH: Update and evaluation. *Journal of Geophysical Research: Atmospheres*, 105(D7):8931–8980, 2000.

D. Taraborrelli, M. G. Lawrence, J. N. Crowley, T. J. Dillon, S. Gromov, C. B. M. Groß, L. Vereecken, and J. Lelieveld. Hydroxyl radical buffered by isoprene oxidation over tropical forests. *Nature Geoscience*, 5(3):190–193, 2012.

K. C. Wells, D. B. Millet, V. H. Payne, M. J. Deventer, K. H. Bates, J. A. de Gouw, M. Graus, C. Warneke, A. Wisthaler, and J. D. Fuentes. Satellite isoprene retrievals constrain emissions and atmospheric oxidation. *Nature*, 585(7824):225–233, 2020.

B. Zheng, F. Chevallier, Y. Yin, P. Ciais, A. Fortems-Cheiney, M. N. Deeter, R. J. Parker, Y. Wang, H. M. Worden, and Y. Zhao. Global atmospheric carbon monoxide budget 2000–2017 inferred from multi-species atmospheric inversions. *Earth System Science Data Discussions*, 2019. https://doi.org/https://doi.org/10.5194/essd-2019-61.